Convective Heat Transfer in Microchannels of Noncircular Cross Sections: An Analytical Approach

S. Shahsavari[1]

A. Tamayol

E. Kjeang

M. Bahrami

Laboratory for Alternative Energy Conversion,
Mechatronic Systems Engineering,
School of Engineering Science,
Simon Fraser University, BC V3T 0A3, Canada

Analytical solutions are presented for velocity and temperature distributions of laminar fully developed flow of Newtonian, constant property fluids in micro/minichannels of hyperelliptical and regular polygonal cross sections. The considered geometries cover several common shapes such as ellipse, rectangle, rectangle with round corners, rhombus, star-shape, and all regular polygons. The analysis is carried out under the conditions of constant axial wall heat flux with uniform peripheral heat flux at a given cross section. A linear least squares point matching technique is used to minimize the residual between the actual and the predicted values on the boundary of the channel. Hydrodynamic and thermal characteristics of the flow are derived; these include pressure drop and local and average Nusselt numbers. The proposed results are successfully verified with existing analytical and numerical solutions from the literature for a variety of cross sections. The present study provides analytical-based compact solutions for velocity and temperature fields that are essential for basic designs, parametric studies, and optimization analyses required for many thermofluidic applications. [DOI: 10.1115/1.4006207]

Keywords: mini/microchannels, fully developed flow, noncircular channels, forced convection

1 Introduction

Advances in microfabrication technologies make it possible to make microchannels with various cross sections in microfluidic devices. The convective flow and heat transfer in these channels, apart from their theoretical interest, are of considerable practical importance for the following applications: microelectronics cooling [1], microelectromechanical systems (MEMS) [2], fuel cell technology [3,4], microreactors [5], and medical and biomedical devices [6]. The developments in the MEMS devices naturally require cooling systems that are equally small. Among the novel methods for thermal management of the high heat fluxes found in microelectronic devices, microchannel heat sinks are the most effective [7]. In addition, porous materials and microchannels filled with porous media can be modeled as networks of microscale conduits with noncircular cross sections [8,9]; thus, transport properties of porous structures are closely related to the geometry of the considered microchannels. A proper understanding of fluid flow and heat transfer in these microscale systems is, therefore, essential for their design and operation.

Several experimental studies have confirmed that the continuum theory holds in micron size channels; see, for example, Refs. [10–13]. Thus, existing solutions for large scale ducts are also applicable to microchannels. Moreover, due to small scales, fully developed condition is achieved very fast in the microchannels [14]. As such, the fully developed assumption is reasonable in the analysis of transport phenomena through microchannels.

The important parameters for design of microchannel chips and their analysis are pressure drop and heat transfer rate. Bahrami et al. [15,16] have developed a general model for predicting pressure drop in microchannels of arbitrary cross section with continuum and slip regimes on channel walls. Recently, Akbari et al.

[17] have extended the model of Refs. [15,16] to arbitrary cross section channels with slowly varying cross sections. Using a similar approach, Sadeghi et al. [18] have reported a general model for estimating the Nusselt number in arbitrary cross section channels. However, these general models do not provide any information about the velocity and temperature distributions.

Accurate information on the velocity and temperature fields are particularly important in devising efficient strategies in a host of engineering applications such as microfluidic, lab-on-chip devices, and fuel cell technologies, to name a few. As such, different methods have been used in the literature to analyze the problem of fully developed laminar flow in noncircular channels, such as analogy method, complex variables method, conformal mapping method, finite difference method, and point matching method [19]. The difficulty for obtaining an analytical solution for this problem by means of the well known classical techniques resides in the impossibility of the separation of variables. An additional difficulty is due to the nonregular two-dimensional characteristics of the cross section.

Sparrow and Haji-Sheikh [20] proposed a method of least squares matching of boundary values for fully developed laminar flow in ducts of arbitrary cross section. It was an improved version of the point matching technique, which was previously employed by Sparrow et al. [21]. Tyagi [22] analyzed the steady laminar forced convection heat transfer in the fully developed flow of liquids through a certain class of channels including equilateral triangular and elliptical tube, using complex variables technique. Shah [23] presented a least squares matching technique to analyze the fully developed laminar fluid flow and heat transfer in ducts of various cross sections. Richardson [24] reported a Leveque solution for flow through elliptical channels. A comprehensive survey of analytical solutions and alternate methods to study such transport phenomena and interpret the results for 25 different geometries, the pertinent literature is published by Shah and London [19]. Abdel-Wahed and Attia [25] evaluated hydrodynamic and thermal characteristics of fully developed laminar flow in an
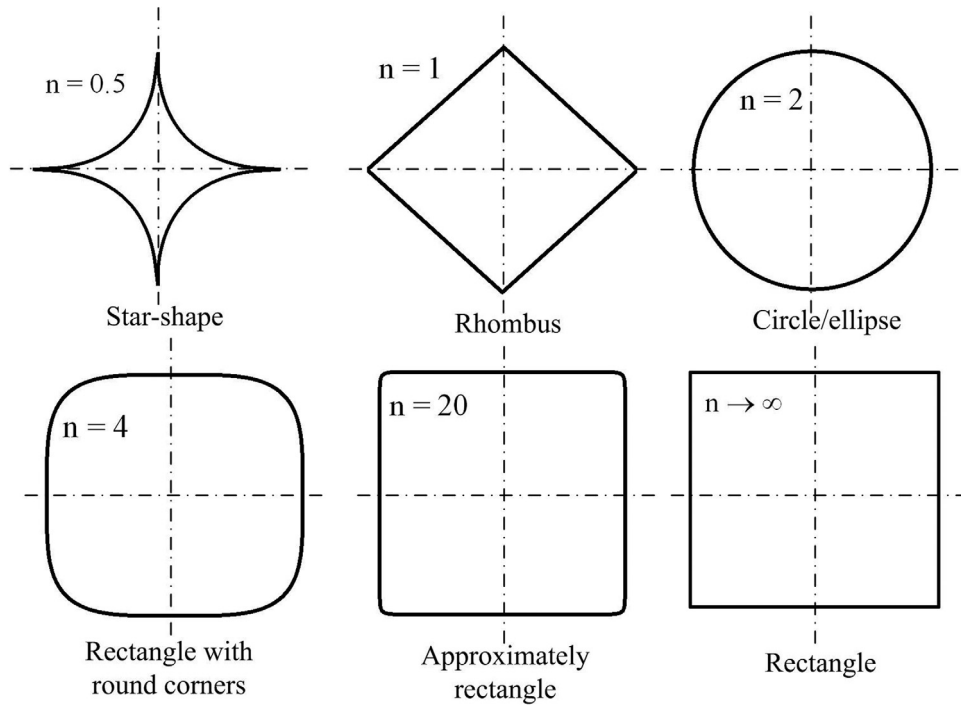
Fig. 1 Hyperelliptical cross sections for $\varepsilon = 1$

arbitrarily shaped triangular duct using a finite difference technique. Maia et al. [26] solved the heat transfer problem in thermally developing laminar flow of a non-Newtonian fluid in elliptical ducts by using the generalized integral transform technique. They transformed the axes algebraically from the Cartesian coordinate system to the elliptical coordinate system in order to avoid the irregular shape of the wall in the elliptical duct. However, this method cannot be used in more complex geometries for which transformation is not possible. In order to develop a general approach applicable to various noncircular geometries, Tamayol and Bahrami [27] employed point matching technique for determining the velocity distribution of fully developed laminar flow in straight channels of regular polygonal and hyperelliptical cross section. However, they did not consider the thermal problem.

In spite of numerous studies available in the literature for pressure drop and Nusselt number, to the best knowledge of authors, velocity and temperature distributions have not been reported in the literature for many of noncircular cross sections. As such, in this study, analytical solutions are presented for velocity and temperature distributions of laminar fully developed flow of Newtonian, constant property fluids through micro/minichannels of both hyperelliptical and polygonal cross-sectional geometries subjected to H2 thermal boundary condition, i.e., constant heat flux boundary condition [19]. To evaluate the convective term in the energy equation, first the momentum equation is solved. Constant heat flux boundary condition is then applied to find the solution of the energy equation for the considered equations. The considered geometries include (i) hyperelliptical channels, encompassing concave/convex shapes from star-shaped, rhombic, elliptical, rectangular with round corners, and rectangular; and (ii) regular polygon ducts, which covers several common shapes from equilateral triangular, squared, pentagonal, hexagonal, and to circular. The proposed solution is presented in a single unique format that covers all the above mentioned cross sections.

2 Problem Statement

Fully developed, steady-state, laminar, constant properties, and incompressible flow in straight micro/minichannels of uniform cross section is studied. In addition, the noncontinuum effects such as slip velocity on the channel walls are neglected. Thus, the present solutions are valid for flow with Knudsen numbers (λ/D_h) less than 0.01, where λ is the molecular mean free path [28,29]. The cross sections investigated in the present study are the hyperellipse and the regular polygon, which will be discussed in details in Sec. 2.1.

2.1 Considered Geometries. In the first quadrant, a hyperellipse is described by

$$r_0 = \frac{a}{\left((\cos\theta)^n + (\sin\theta/\varepsilon)^n\right)^{1/n}}, \quad 0 < \varepsilon = \frac{b}{a} \leq 1 \quad (1)$$

where ε is the aspect ratio, a and b are the major and minor axes of the cross section, respectively. As shown in Fig. 1, by varying parameter n, several geometries can be created. For examples, Eq. (1) with $n = 0.5$ results in a star-shaped geometry. $n = 1$ results in a rhombus and when $n = 2$ yields an ellipse; for $a = b$, the consequent geometry is a circle. For $n > 2$, a rectangle with round corners is created and when the resulting geometry becomes a rectangle; in the special case of $a = b$, it represents a square and for $a \ll b$, it yields parallel plates. It should be noted that as a result of manufacturing processes, some of the flow passages have round corners; thus rectangle with round corner can be observed in many practical applications. The cross-sectional area of a hyperellipse can be expressed in terms of the gamma function, $\Gamma(x)$, [30]

$$A = 4^{1-1/n} a^2 \varepsilon \sqrt{\pi} \frac{\Gamma\left(1 + \frac{1}{n}\right)}{\Gamma\left(\frac{1}{2} + \frac{2}{n}\right)} \quad (2)$$

The perimeter of the hyperellipse does not have a closed form solution and must be calculated from the following integral:

$$\Gamma_c = 4 \int_0^{\pi/2} \sqrt{\left(\frac{dr_0}{d\theta}\right)^2 + r_0^2} \, d\theta \quad (3)$$
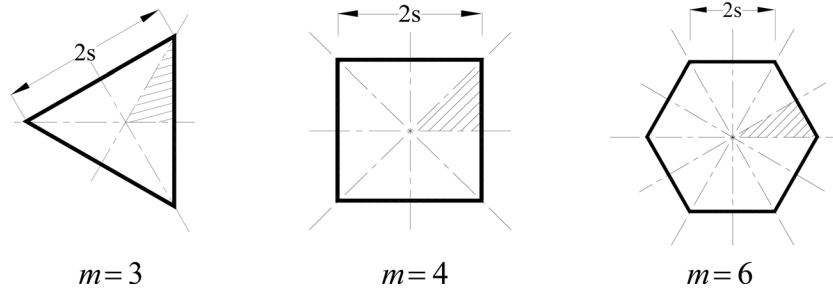
Fig. 2 Regular polygons with different number of sides

As shown in Fig. 2, the m-sided regular polygon ducts covers a wide range of geometries. For $m = 3$, the consequent geometry is an equilateral triangle; when $m = 4$ and 6 the shapes become a square and a hexagon, respectively. A circle is a polygon with infinite number of sides, i.e., $m \rightarrow \infty$. As shown in Fig. 2, all the hatched regions surrounded by symmetry lines are triangles with different vertex angles.

3 Problem Formulation

3.1 Momentum Equation. The liquid flow in minichannels and microchannels in the absence of any wall surface effects, such as the electrokinetic or electroosmotic forces, is not expected to experience any fundamental deviation from the continuum theory employed in microfluidic applications [31]. Gad-el-Hak [32] argued that liquids such as water should be treated as continuous media with the results obtained from classical theory being applicable in channels larger than 1 μm.

The compressibility effects can be neglected for the Mach numbers lower than 0.3 [33]; thus, the present analysis is acceptable for all Newtonian liquids and gas flows with Ma < 0.3. For laminar flow with negligible gravitational effects subjected to the abovementioned assumptions, momentum equation reduces to the Poisson's equation [33]

$$\frac{dP}{dz} = \mu \left(\frac{\partial^2 u}{\partial r^2} + \frac{1}{r} \frac{\partial u}{\partial r} + \frac{1}{r^2} \frac{\partial^2 u}{\partial \theta^2} \right) \quad (4)$$

where μ is the fluid viscosity, P is pressure, and u is the fluid velocity along the channel axis. Using the geometrical symmetry, only a portion of the cross section is considered in the analysis, as shown in Fig. 3. Applicable boundary conditions for hyperelliptical channels are

$$\left. \frac{\partial u}{\partial \theta} \right|_{\theta = \frac{\pi}{2}} = 0, \quad \left. \frac{\partial u}{\partial \theta} \right|_{\theta = 0} = 0, \quad u(r_0) = 0 \quad (5)$$

The first two equations are obtained from the existing symmetry in the hyperellipse geometry. The general solution of the Poisson's equation, Eq. (4), in the cylindrical coordinate system is [34]

$$u = A_0 + B \ln r - \frac{r^2}{4\mu} \left(\frac{dP}{dz} \right)$$

$$+ \sum_{k=1}^{\infty} \left(C_k r^k + D_k r^{-k} \right) \left(E_k \cos k\theta + F_k \sin k\theta \right) \quad (6)$$

The unknown coefficients A_0, B, C_k, D_k, E_k, and F_k should be calculated through applying the boundary conditions, Eq. (5). At $r = 0$, the velocity must have a finite value; thus, $B = D_k = 0$. Since dP/dz remains constant for fully developed flows, Eq. (6) can be simplified as
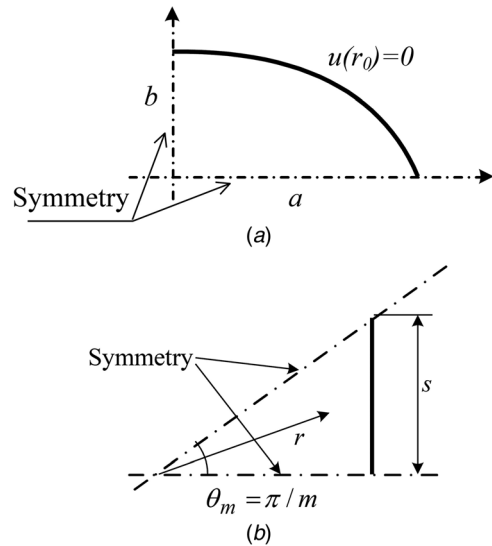

Fig. 3 Considered geometry for modeling (a) hyperelliptical and (b) regular polygonal cross section and the applied boundary conditions

$$u = \frac{1}{\mu} \left(-\frac{dP}{dz} \right) \left[A_1 - \frac{r^2}{4} + \sum_{k=1}^{\infty} \left(r^k \right) \left(E_k \cos k\theta + F_k \sin k\theta \right) \right] \quad (7)$$

where A_1, E_k, and F_k are redefined. The symmetry conditions at $\theta = 0$ and $\theta = \pi/2$ result in $F_k = 0$ and $k = 2, 4, 6, \ldots$, respectively. After nondimensionalizing, Eq. (7) reduces to

$$u^* = A_1 - \frac{\eta^2}{4} + \sum_{i=1}^{\infty} C_i \left(\eta^{2i} \cos 2i\theta \right),$$

$$u^* = \frac{u}{\frac{1}{\mu} \left(-\frac{dP}{dz} \right) a^2}, \quad \eta = \frac{r}{L_c} = \frac{r}{a} \quad (8)$$

The last boundary condition, i.e., the no-slip condition, $u^*(\eta_0) = 0$, on the channel wall should be used to calculate the rest of unknown coefficients in Eq. (8). Substituting for η_0 from Eq. (1), one can write

$$A_1 - \frac{1}{4} \frac{1}{\left((\cos \theta)^n + (\sin \theta / \varepsilon)^n \right)^{2/n}}$$

$$+ \sum_{i=1}^{\infty} C_i \left(\frac{\cos 2i\theta}{\left((\cos \theta)^n + (\sin \theta / \varepsilon)^n \right)^{2i/n}} \right) = 0 \quad (9)$$

This equation is a function of θ. To evaluate the coefficients, following Ref. [23], we truncate the series from the q th term and

apply Eq. (9) over a finite number of different θ s and solve the resulting set of linear equations.

The same approach can be followed for polygonal ducts, shown in Fig. 3. The difference between the two geometries is the location of the symmetry lines. The applicable symmetry boundary conditions for the polygonal cross section are

$$\frac{\partial u}{\partial \theta}\bigg|_{\theta=\frac{\pi}{m}} = 0, \qquad \frac{\partial u}{\partial \theta}\bigg|_{\theta=0} = 0 \qquad (10)$$

where m is the number of sides. Using Eq. (10), the dimensionless velocity distribution becomes

$$u^* = A_1 - \frac{\eta^2}{4} + \sum_{i=1}^{\infty} C_i \left(\eta^{mi} \cos m\theta \right),$$

$$u^* = \frac{u \left(\tan \frac{\pi}{m} \right)^2}{\frac{1}{\mu} \left(-\frac{dP}{dz} \right) s^2}, \qquad \eta = \frac{r}{L_c} = \frac{r \tan \frac{\pi}{m}}{s} \qquad (11)$$

Applying no-slip boundary condition, the unknown coefficients in Eqs. (8) and (11) can be determined.

One of the techniques that can be employed to apply the no-slip boundary is the point matching technique [21,27,35,36]. In this approach, the infinite series can be truncated at a finite number of terms, q. Then, $q + 1$ points are selected on the periphery and the boundary condition is satisfied exactly at these $q + 1$ points to determine the same number of unknown coefficients of the truncated series. The velocity and temperature distributions are then obtained in a closed-form series. The limitation of this method is that by increasing the number of points on the boundary, one cannot necessarily obtain a more accurate result since the degree of the polynomial is increased, which may result in overfitting. Using point-matching technique, Tamayol and Bahrami [27] could not predict the velocity distribution and pressure drop for concave geometries such as star-shaped channels. To overcome this limitation, the least squares method is used in the present study. It should be noted that the pressure drop values for convex geometries reported by Tamayol and Bahrami [27] were the same as the results reported by Shah and London [19] and predicted by the least squares method in the present study.

The least squares method differs from the point-matching method in that more than q points along the boundary are employed to determine q unknown coefficients in the truncated series. Therefore, we will have an overdetermined linear system of equations. The coefficients are evaluated by minimizing the mean squared error of the boundary conditions at j points ($j > q$) [37]. It should be noted that increasing the number of terms, q, in the series solution does not guarantee more accuracy and it depends on the nature of the series solution. For each geometry, we performed a comprehensive study to select the number of terms in the series solution which yielded the minimum error in satisfying the wall boundary conditions; two or three terms for most cases. Moreover, the number of points on the channel wall, j, were in the range of 200–250.

3.2 Energy Equation. In addition to idealizations made for the momentum equation, for simplifying the energy equation, axial heat conduction is neglected, following Ref. [38]. This term is negligible when Péclet number, which measures the ratio of the bulk transport (convection) to the diffusion transport, is high (see Ref. [28] for more details). Moreover, in continuum and slip-flow regimes, viscous dissipation is negligible. Viscous heat generation is significant in extremely viscous liquids or gas flows with relatively high velocity and temperature gradients [39]. Thus, the energy equation for laminar hydrodynamically and thermally developed flow becomes

$$\frac{u}{\alpha} \frac{\partial T}{\partial z} = \frac{\partial^2 T}{\partial r^2} + \frac{1}{r} \frac{\partial T}{\partial r} + \frac{1}{r^2} \frac{\partial^2 T}{\partial \theta^2} \qquad (12)$$

where α is thermal diffusivity of the fluid. The associated thermal boundary condition is considered as axially constant heat transfer rate per unit channel length, with peripherally uniform heat flux. For this boundary condition and fully developed flow, it can be shown that [40]

$$\frac{\partial T}{\partial z} = \frac{dT_m}{dz} = \frac{q'' \Gamma_c}{\rho A_c u_m c_p} \qquad (13)$$

where c_p is the specific heat of fluid, A_c is the channels cross section, Γ_c is the cross section perimeter, u_m and T_m are the mean velocity and temperature, respectively, defined as

$$u_m = \frac{\int_{A_c} u \, dA_c}{A_c}, \qquad T_m = \frac{\int_{A_c} uT \, dA_c}{u_m A_c} \qquad (14)$$

Substituting Eqs. (12) and (7) into Eq. (13) yields

$$\frac{\partial^2 T}{\partial r^2} + \frac{1}{r} \frac{\partial T}{\partial r} + \frac{1}{r^2} \frac{\partial^2 T}{\partial \theta^2}$$
$$= \frac{1}{\mu} \left(\frac{dP}{dz} \right) \left[A_1 - \frac{r^2}{4} + \sum_{k=1}^{\infty} \left(r^k \right) \left(E_k \cos k\theta + F_k \sin k\theta \right) \right]$$
$$\times \frac{q'' \Gamma_c}{\rho \alpha A_c u_m c_p} \qquad (15)$$

which in the dimensionless form for hyperelliptical cross section becomes

$$\frac{\partial^2 T^*}{\partial \eta^2} + \frac{1}{\eta} \frac{\partial T^*}{\partial \eta} + \frac{1}{\eta^2} \frac{\partial^2 T^*}{\partial \theta^2} = \left[1 - \frac{\eta^2}{4A_1} + \sum_{i=1}^{\infty} \frac{C_i}{A_1} \left(\eta^{2i} \cos 2i\theta \right) \right] \qquad (16)$$

and for regular polygonal cross section reads

$$\frac{\partial^2 T^*}{\partial \eta^2} + \frac{1}{\eta} \frac{\partial T^*}{\partial \eta} + \frac{1}{\eta^2} \frac{\partial^2 T^*}{\partial \theta^2} = \left[1 - \frac{\eta^2}{4A_1} + \sum_{i=1}^{\infty} \frac{C_i}{A_1} \left(\eta^{mi} \cos mi\theta \right) \right] \qquad (17)$$

and where T^* is defined as

$$T^* = \frac{T}{\frac{q'' \Gamma_c L_c^2}{\rho \alpha A_c u^* c_p}} \qquad (18)$$

where L_c is the cross-sectional length-scale, introduced in Eqs. (8) and (11) for hyperelliptical and polygonal cross sections, respectively. As discussed by Sparrow and Loeffler [36], the solution of Eq. (15) is expressed as the sum of separate particular and homogeneous solutions as follows:

$$T^* = T_p^* + T_h^* \qquad (19)$$

The particular solution is [34]

$$T_p^* = \begin{cases} A_1 \dfrac{\eta^2}{4} - \dfrac{\eta^4}{64} + \displaystyle\sum_{i=1}^{\infty} \dfrac{C_i}{4(2i+1)} \left(\eta^{2i+2} \cos 2i\theta \right) & \text{hyperellipse} \\[4ex] A_1 \dfrac{\eta^2}{4} - \dfrac{\eta^4}{64} + \displaystyle\sum_{i=1}^{\infty} \dfrac{C_i}{4(mi+1)} \left(\eta^{mi+2} \cos mi\theta \right) & \text{polygon} \end{cases} \qquad (20)$$

Table 1 Velocity and temperature distribution coefficients in Eqs. (8) and (23) for hyperelliptical channels

	$\varepsilon=0.2$	$\varepsilon=0.25$	$\varepsilon=0.4$	$\varepsilon=0.5$	$\varepsilon=0.6$	$\varepsilon=0.8$	$\varepsilon=1$
			$n=40$, Rectangle				
A_1	0.0198	0.0309	0.0768	0.1141	0.1533	0.2293	0.2948
C_1	0.2600	0.2617	0.2401	0.2062	0.1649	0.0781	0.0000
C_2	-0.0250	-0.0369	-0.0617	-0.0665	-0.0657	-0.0577	-0.0479
d_1	-0.0068	-0.0083	-0.0084	-0.0078	-0.0069	-0.0040	0.000
d_2	-0.0013	-0.0003	0.0000	0.0000	0.0000	0.0000	0.0028
			$n=4$, Rectangle with round corner				
A_1	0.0199	0.0309	0.0755	0.1116	0.1495	0.2231	0.2867
C_1	0.2508	0.2475	0.2192	0.1874	0.1499	0.0712	0.000
C_2	-0.0188	-0.0259	-0.0413	-0.0454	-0.0459	-0.0415	-0.0347
d_1	-0.0076	-0.0088	-0.0088	-0.0085	-0.0077	-0.0046	0.000
d_2	-0.0009	0.0000	0.0000	0.0000	0.0000	0.0000	0.0028
			$n=2$, Ellipse				
A_1	0.0192	0.0294	0.0690	0.1000	0.1324	0.1951	0.250
C_1	0.2308	0.2206	0.1810	0.1500	0.1176	0.0549	0
d_1	-0.0080	-0.0065	-0.0083	-0.0082	-0.0075	-0.0046	0
			$n=1$, Rhomboid				
A_1	0.0151	0.0222	0.0470	0.0647	0.0824	0.1164	0.1474
C_1	0.1980	0.1769	0.1161	0.0833	0.0578	0.0230	0.0000
C_2	0.0421	0.0580	0.0979	0.1133	0.1196	0.1137	0.0963
d_1	-0.0025	-0.0029	0.0000	0.0000	0.0000	0.0000	0.0000
			$n=0.5$, Star-shape				
A_1	0.1282	0.1073	0.0853	0.0631	0.0424	0.0245	0.0115
C_1	0.0000	0.0000	0.0000	0.0000	0.0000	0.0000	0.0000
C_2	0.1191	0.1476	0.1831	0.2267	0.2708	0.2778	0.2520
d_1	0.0000	0.0000	0.0000	0.0000	0.0000	0.0000	0.0000

and the general homogeneous solution becomes

$$T_h^* = d_0 + \sum_{j=1}^{\infty} \eta^j \left(d_j \cos j\theta + e_j \sin j\theta \right) \qquad (21)$$

Appling the symmetry boundary conditions, we obtain: $e_j = 0$ and $j = 2, 4, \ldots$ and $j = m, 2m, \ldots$ for elliptical and polygonal cross sections, respectively. Thus, Eq. (21) can be written as

Table 2 Velocity and temperature distribution coefficients in Eqs. (11) and (23) for polygonal channels

m	A_1	C_1	C_2	d_1
3	0.0833	-0.1667	0	0
4	0.1473	-0.0909	0.0103	0
5	0.1823	-0.0558	0.0095	0
6	0.2024	-0.0374	0.0075	0
7	0.2149	-0.0267	0.0058	0.0006
8	0.2231	-0.0199	0.0046	0.0004
9	0.2288	-0.0154	0.0036	0.0003
10	0.2328	-0.012	0.003	0.0002
20	0.2458	-0.0028	0.0007	0

$$T_h^* = \begin{cases} d_0 + \sum_{j=1}^{\infty} \eta^{2j} \left(d_j \cos 2j\theta \right) & \text{hyperellipse} \\ d_0 + \sum_{j=1}^{\infty} \eta^{mj} \left(d_j \cos mj\theta \right) & \text{polygon} \end{cases} \qquad (22)$$
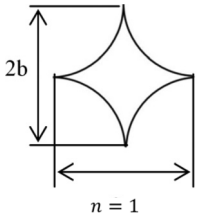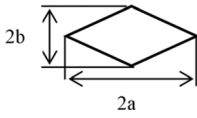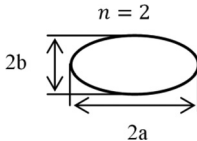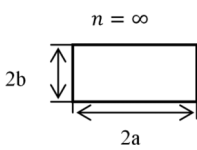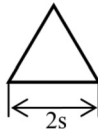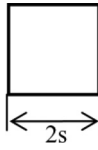
Therefore, the temperature distribution becomes

$$T^* = \begin{cases} A_1 \dfrac{\eta^2}{4} - \dfrac{\eta^4}{64} + \sum_{i=1}^{\infty} \dfrac{C_i}{4(2i+1)} \left(\eta^{2i+2} \cos 2i\theta \right) + \\ \quad d_0 + \sum_{j=1}^{\infty} \eta^{2j} \left(d_j \cos 2j\theta \right) \qquad \text{hyperellipse} \\ A_1 \dfrac{\eta^2}{4} - \dfrac{\eta^4}{64} + \sum_{i=1}^{\infty} \dfrac{C_i}{4(mi+1)} \left(\eta^{mi+2} \cos m\theta \right) + \\ \quad d_0 + \sum_{j=1}^{\infty} \eta^{mj} \left(d_j \cos mj\theta \right) \qquad \text{polygon} \end{cases}$$

$$(23)$$

The unknown coefficients should be determined through applying the constant heat flux per unit area on the channel wall

$$\left. \frac{\partial T^*}{\partial n} \right|_{\eta=\eta_0} = \frac{A_c^* \, u_m^*}{\Gamma_c^*} \qquad (24)$$

Table 3 Examples of the present solution for fully developed velocity and temperature distributions

| Cross section	Aspect ratio	Velocity profile (u^*)	Temperature profile ($\bar{T} = T^* - T_b^*$)
(star shape, $2b$, $n=1$)	$\varepsilon = 1$	$0.0424 - \frac{1}{4}\eta^2$ $+ 0.2708\eta^4 \cos 4\theta$	$-0.0009 + 0.0106\eta^2 - \frac{\eta^4}{64}$ $+ 0.0135\eta^6 \cos 4\theta$
(diamond, $2b$, $2a$, $n=2$)	$\varepsilon = 0.5$	$0.0647 - \frac{1}{4}\eta^2$ $+ 0.0833\eta^2 \cos 2\theta$ $+ 0.1133\eta^4 \cos 4\theta$	$-0.0014 + 0.0162\eta^2 - \frac{\eta^4}{64}$ $+ 0.0069\eta^4 \cos 2\theta$ $+ 0.0057\eta^6 \cos 4\theta$
(ellipse, $2b$, $2a$, $n=\infty$)	$\varepsilon = 0.5$	$0.1 - \frac{1}{4}\eta^2 + 0.15\eta^2 \cos 2\theta$	$-0.0037 + \frac{\eta^2}{40} - \frac{\eta^4}{64}$ $- 0.0082\eta^2 \cos 2\theta$ $+ 0.0075\eta^4 \cos 2\theta$
(rectangle, $2b$, $2a$)	$\varepsilon = 0.5$	$0.1141 - \frac{1}{4}\eta^2$ $+ 0.2062\eta^2 \cos 2\theta$ $- 0.0665\eta^4 \cos 4\theta$	$-0.0057 + 0.1141\frac{\eta^2}{4} - \frac{\eta^4}{64}$ $- 0.0078\eta^2 \cos 2\theta$ $+ 0.2062\frac{\eta^4}{12}\cos 2\theta$ $- 0.0665\frac{\eta^6}{20}\cos 4\theta$
(triangle, $2s$)	—	$0.0833 - \frac{1}{4}\eta^2$ $- 0.1667\eta^3 \cos 3\theta$	$-0.0024 + 0.0208\eta^2 - \frac{\eta^4}{64}$ $- 0.0104\eta^5 \cos 3\theta$
(square, $2s$)	—	$0.1473 - \frac{1}{4}\eta^2$ $- 0.0909\eta^4 \cos 4\theta$ $+ 0.0103\eta^8 \cos 8\theta$	$-0.0067 + 0.1473\frac{\eta^2}{4} - \frac{\eta^4}{64}$ $- 0.0909\frac{\eta^6}{20}\cos 4\theta$ $+ 0.0103\frac{\eta^{10}}{36}\cos 8\theta$
(pentagon, $2s$)	—	$0.1823 - \frac{1}{4}\eta^2$ $- 0.0558\eta^5 \cos 5\theta$ $+ 0.0095\eta^{10}\cos 10\theta$	$-0.0099 + 0.1823\frac{\eta^2}{4} - \frac{\eta^4}{64}$ $- 0.0558\frac{\eta^7}{24}\cos 5\theta$ $+ 0.0095\frac{\eta^{12}}{44}\cos 10\theta$
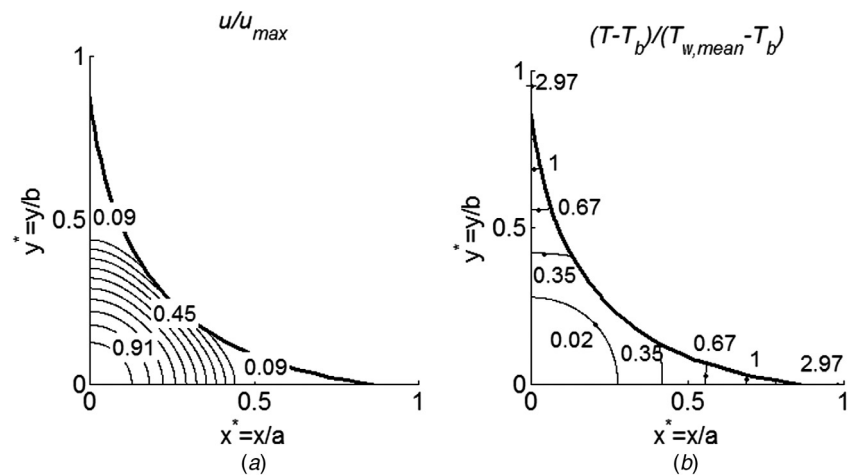
Fig. 4 Dimensionless velocity and temperature contours in a star-shaped channel with = 0.5 and = 1, using (a) Eq. (8) and (b) Eq. (23)
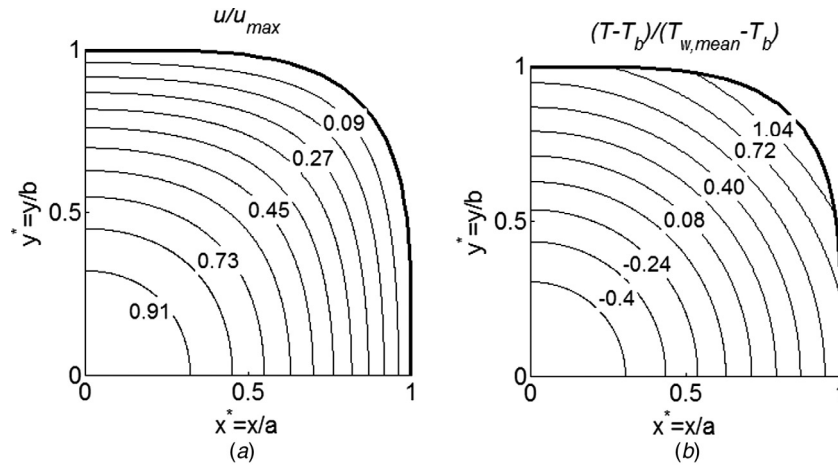
Fig. 5 Dimensionless velocity and temperature contours in a square with round corners duct, = 4, using (a) Eq. (8) and (b) Eq. (23)
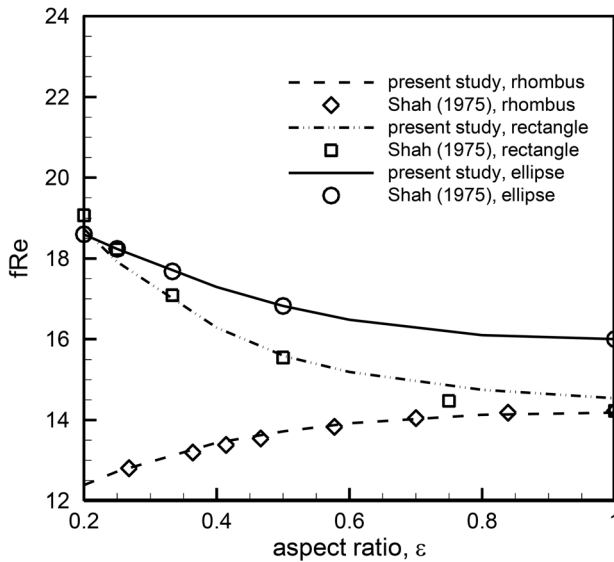

Fig. 6 Comparison of the values of Poiseuille number in channels of hyperelliptical cross section calculated using the present model with numerical results of Shah [23]
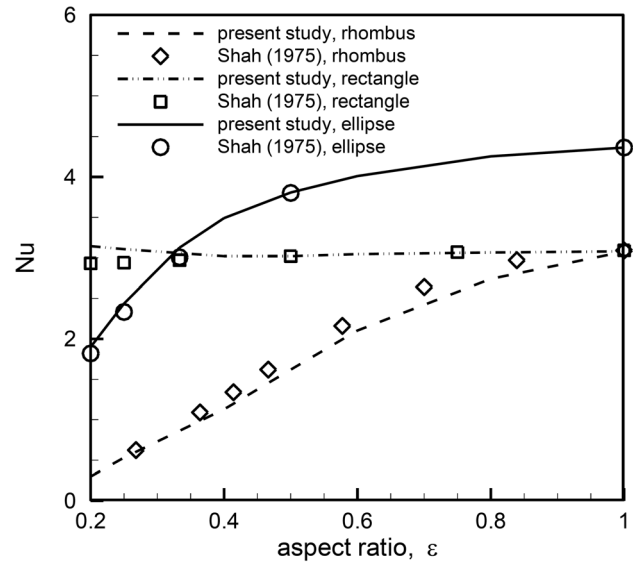

Fig. 7 Comparison of the values of Nusselt number in channels of hyperelliptical cross section calculated using the present model with numerical results of Shah [23]

where A_c^* and Γ_c^* are dimensionless perimeter and cross-sectional area defined as $A_c^* = A_c/L_c^2$ and $\Gamma_c^* = \Gamma_c/L_c$. The normal gradient of temperature is

$$\frac{\partial T^*}{\partial n} = \hat{n}.\vec{\nabla}T^* \qquad (25)$$

where $\hat{n}$ is the normal vector of the boundary defined by $F(\eta, \theta) = 0$

$$F(\eta, \theta) = \begin{cases} \eta\left[(\cos\theta)^n + \left(\dfrac{\sin\theta}{\varepsilon}\right)^n\right]^{1/n} - 1 & \text{hyperellipse} \\ \eta\cos\theta - \cos(\pi/m) & \text{polygon} \end{cases}$$

$$(26)$$

Using a similar approach employed to solve the momentum equation, the infinite series in Eq. (23) is truncated. The coefficients d_j are calculated by the least squares point matching technique.

4 Results and Discussions

In order to calculate velocity and temperature distributions, the coefficient in Eqs. (8), (11) and (23) should be determined. Therefore, a least squares point matching technique has been employed and the calculated coefficients are reported in Tables 1 and 2. Considering just the first two terms of the infinite series in the solutions to the velocity and temperature distributions resulted in an average error of less than 1% in applying the boundary value for the various geometries that were studied in this work. As an example, Table 3 shows the closed form velocity and temperature relations for some examples from the studied geometries. It should be mentioned that the velocity and temperature solutions for star-shaped and rectangular-with-round-corners channels cannot be found elsewhere. The former one has application in analyzing foams and packed beds of fibers and the later one is common in micro fabrication process of rectangular microchannels. Some examples of the velocity contours and distributions are plotted for ducts with star-shaped and square with round corners cross sections in Figs. 4 and 5, respectively.
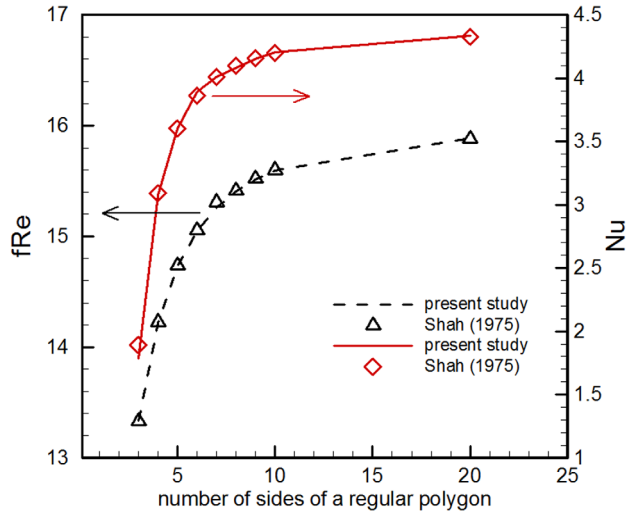
Fig. 8 Comparison of the values of Poiseuille number and Nusselt number in channels of polygonal cross section calculated using the present model with numerical results of Shah [23]

Two important characteristics of convective flow in channels are the Poiseuille number and the Nusselt number. The Poiseuille number, $f\,\mathrm{Re}$, is the common dimensionless number used for analyzing pressure drop in channels and is defined by

$$f\,\mathrm{Re} = -\frac{1}{\mu}\frac{dP}{dz} \times \frac{D_h^2}{2u_m} \qquad (27)$$

where D_h is the hydraulic diameter. The Nusselt number, Nu is the ratio of convective to conductive heat transfer normal to the boundary. The local Nusselt number is defined by

$$\mathrm{Nu} = \frac{D_h}{T_w - T_b}\frac{\partial T}{\partial n}\bigg|_{r=r_o} \qquad (28)$$

where T_w is the wall temperature and T_b is the fluid bulk temperature defined as

$$T_b = \frac{\displaystyle\int_{A_c} uT\,dA_c}{\displaystyle\int_{A_c} u\,dA_c} \qquad (29)$$

The average Nusselt number is defined by using the average wall temperature in Eq. (28). The results for the Poiseuille number and Nusselt number are plotted in Figs. 6 and 7 for hyperelliptical channels and Fig. 8 for polygonal ducts and are compared with analytical/numerical data found in the literature [19,23]. It can be seen that the proposed approach is in a very good agreement with the numerical data and the deviations between the model and the numerical results less are less than 3%.

It should be noted that a cross section with a higher $f\,\mathrm{Re}$ and Nu does not essentially result in higher pressure drop or heat transfer rate. For example, although circular cross section has the highest $f\,\mathrm{Re}$ among polygonal channels as shown in Fig. 8, it results in the lowest pressure drop.

Tamayol and Bahrami [27] provided a compact relationship for $f\,\mathrm{Re}$; however, the following equation is more compact and can accurately predict $f\,\mathrm{Re}$ for all polygonal channels:

$$f\,\mathrm{Re} = -13.017m^{-1.407} + 16 \qquad (30)$$

No compact relationship was found for the Nusselt number in the pertinent literature. As such, a similar relationship is proposed for
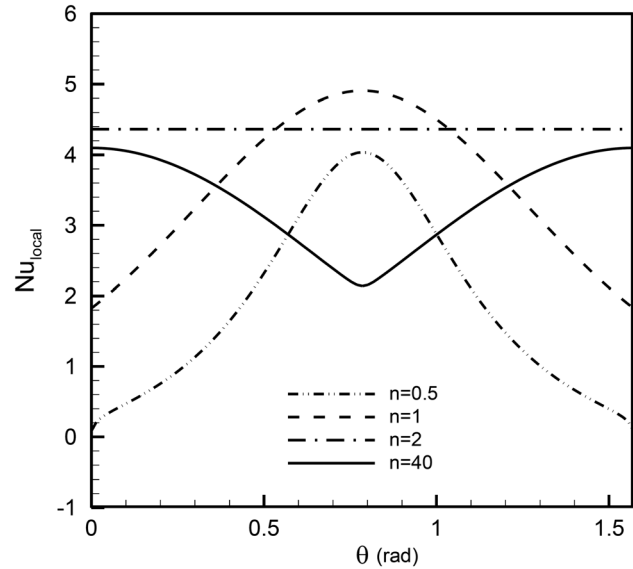

Fig. 9 Variation of the local Nusselt number in channels of hyperelliptical cross section, $\varepsilon = 1$

determining the Nusselt number in regular polygonal channels subjected to H2 thermal boundary condition

$$\mathrm{Nu} = -36.688m^{-2.425} + 4.36 \qquad (31)$$

Equations (30) and (31) can predict $f\,\mathrm{Re}$ and Nu values for polygonal ducts with uncertainty less than 2%, respectively.

In Fig. 9, the local Nusselt number, calculated from Eq. (31), is plotted for channels with hyperelliptical cross section. The results indicate that Nusselt number varies over the periphery of the channel with a minimum at the corners. For geometries with $n < 2$, the corners are located at $\theta = 0$, $\pi/2$ and the maximum value of Nu_{local} occurs at $\theta = \pi/4$. In circular tubes, $n = 2$, Nusselt number is uniformly distributed since no corner exists. For convex geometries with $n > 2$, corners are located at $\theta = \pi/4$ and as a result, Nu_{local} have a minimum at $\theta = \pi/4$.

5 Summary and Conclusions

Analytical solutions were presented for laminar fully developed flow and heat transfer in micro/minichannels of different noncircular cross sections. Starting from general solution of the Poisson's equation, a least squares point matching technique was used for applying the wall boundary conditions in order to minimize the error of the boundary values.

Velocity and temperature distributions were obtained for various geometries with different shapes and aspect ratios, from which hydrodynamic and thermal characteristics of the flow were calculated. The considered geometries encompassed a wide range of shapes such as ellipse, rectangle, rectangle with round corners, rhombus, star-shape, and all regular polygons. However, this approach is applicable to all geometries with at least two symmetry lines. Therefore, the present approach can be considered as a general solution. The compact solutions were obtained by truncating the infinite series in the solutions to the velocity and temperature distributions from the second or third term. The Nusselt and Poiseuille numbers were compared with the published data of Refs. [19,23] for the considered channels, which resulted in a relative difference of less than 3%.

Also, using this method, the local Nusselt numbers were determined. For star-shaped channels, the local Nusselt number near the corners is close to zero, which is a consequence of the relatively low velocity in these regions due to the high wall shear stress. The present compact solutions for the velocity and

temperature distributions provide a powerful tool for design, parametric studies, and optimization analyses required for microchannel heat exchangers, heat sinks, fuel cell technology, and microfluidic devices.

Nomenclature

a = hyperellipse major axis, m
A_c = cross-sectional area, m^2
b = hyperellipse minor axis, m
c_p = specific heat, J/K kg
D_h = hydraulic diameter, $4A/\Gamma_c$, m
f = fanning friction factor
$f\,Re$ = Poiseuille number
I_p = polar moment of inertia about the centroid, m^4
k = thermal conductivity, W/K m
L_c = characteristic length-scale, m^4
m = number of sides in regular polygonal ducts
n = exponent in hyperellipse formula
Nu = Nusselt number
P = pressure, N/m^2
Q = volumetric flow rate, m^3/s
Re = Reynolds number
s = half the length of the sides in polygonal ducts, m
T = temperature, K
T^* = dimensionless temperature
u = axial velocity, m/s
u^* = dimensionless velocity, Eq. (8)

Greek Symbols

$\Gamma(.)$ = gamma function
Γ_c = perimeter, m
ε = cross-sectional aspect ratio, $\varepsilon = b/a$
η = nondimensional coordinate
μ = viscosity, N s/m^2
θ = coordinate system
θ_m = half of the vertex angle in polygon with m sides

Subscripts

$\sqrt{A}$ = square root of cross-sectional area,
w = wall
b = bulk
a = hyperellipse major axis, m
A_c = cross-sectional area, m^2
b = hyperellipse minor axis, m
c_p = specific heat, J/K kg
D_h = hydraulic diameter, $4A/\Gamma_c$, m
f = fanning friction factor
$f\,Re$ = Poiseuille number
k = thermal conductivity, W/K m
I_p = polar moment of inertia about the centroid, m^4
m = number of sides in regular polygonal ducts
n = exponent in hyperellipse formula
Nu = Nusselt number
P = pressure, N/m^2
Q = volumetric flow rate, m^3/s
Re = Reynolds number
s = half the length of the sides in polygonal ducts, m
T = temperature, K
T^* = dimensionless temperature
u = axial velocity, m/s
u^* = dimensionless velocity, Eq. (8)

References

[1] Tuckerman, D. B., and Pease, R. F. W., 1981, "High Performance Heat Sinking for VLSI," IEEE Electron Device Lett., **2**(8), pp. 213–213.
[2] Ho, C. M., and Tai, Y. C., 1998, "Micro-Electro-Mechanical-Systems (MEMS) and Fluid Flows," Annu. Rev. Fluid Mech., **30**(1), pp. 579–612.
[3] Lee, J., and Kjeang, E., 2010, "A Perspective on Microfluidic Biofuel Cells," Biomicrofluidics, **4**(4), p. 041301.
[4] Kjeang, E., Michel, R., Harrington, D. A., Djilali, N., and Sinton, D., 2008, "A Microfluidic Fuel Cell With Flow-Through Porous Electrodes," J. Am. Chem. Soc., **130**(12), pp. 4000–4006.
[5] Gunther, A., Khan, S. A., Thalmann, M., Trachsel, F., and Jensen, K. F., 2004, "Transport and Reaction in Microscale Segmented Gas-Liquid Flow," Lab Chip, **4**(4), pp. 278–286.
[6] Effenhauser, C. S., Manz, A., and Widmer, H. M., 1993, "Glass Chips for High-Speed Capillary Electrophoresis Separations With Submicrometer Plate Heights," Anal. Chem., **65**(19), pp. 2637–2642.
[7] Sobhan, C. B., and Garimella, S. V., 2001, "A Comprehensive Analysis of Studies on Heat Transfer and Fluid Flow in Microchannels," Microscale Thermophy. Eng., **5**, pp. 293–311.
[8] Tamayol, A., and Bahrami, M., 2009, "Analytical Determination of Viscous Permeability of Fibrous Porous Media," Int. J. Heat Mass Transfer, **52**(9-10), pp. 2407–2414.
[9] Tamayol, A., Kholsa, A., Gray, B., and Bahrami, M., 2010, "Pressure Drop in Micro-Channels filled With Porous Media," ICNMM2010, Montreal, Canada.
[10] Pfahler, J., Harley, J., Bau, H., and Zemel, J., 1989, "Liquid Transport in Micron and Submicron Channels," Sens. Actuators, A, **22**(1-3), pp. 431–434.
[11] Harley, J. C., Huang, Y., Bau, H. H., and Zemel, J. N., 1995, "Gas Flow In Micro-Channels," J. Fluid Mech., **284**, pp. 257–274.
[12] Cao, B., Chen, G. W., and Yuan, Q., 2005, "Fully Developed Laminar Flow and Heat Transfer in Smooth Trapezoidal Microchannel," Int. Commun. Heat Mass Transfer, **32**(9), pp. 1211–1220.
[13] Gao, P., Person, S. L., and Favre-Marinet, M., 2002, "Scale Effects on Hydrodynamics and Heat Transfer in Two-Dimensional Mini and Microchannels," Int. J. Therm. Sci., **41**(11), pp. 1017–1027.
[14] Akbari, M., Sinton, D., and Bahrami, M., 2009, "Pressure Drop in Rectangular Microchannels as Compared With Theory Based on Arbitrary Cross Section," ASME J. Fluids Eng., **131**(4), p. 041202.
[15] Bahrami, M., Tamayol, A., and Taheri, P., 2009, "Slip-Flow Pressure Drop in Microchannels of General Cross Section," ASME J. Fluids Eng., **131**(3), p. 031201.
[16] Bahrami, M., Yovanovich, M. M., and Culham, J. R., 2006, "Pressure Drop of Fully-Developed, Laminar Flow in Microchannels of Arbitrary Cross-Section," ASME J. Fluids Eng., **128**(5), pp. 1036–1044.
[17] Akbari, M., Sinton, D., and Bahrami, M., 2011, "Viscous Flow in Variable Cross-Section Microchannels of Arbitrary Shapes," Int. J. Heat Mass Transfer, **54**, pp. 3970–3978.
[18] Sadeghi, E., Bahrami, M., and Djilali, N., 2010, "Estimation of Nusselt Number in Microchannels of Arbitrary Cross Section With Constant Axial Heat Flux," Heat Transfer Eng., **31**(8), pp. 666–674.
[19] Shah, R. K., and London, A. L., 1978, *Laminar Flow Forced Convection in Ducts*, Academic Press, New York.
[20] Sparrow, E. M., and Haji-Sheikh, A., 1965, "Laminar Heat Transfer and Pressure Drop in Isosceles Triangular, Right Triangular and Circular Sector Ducts," ASME J. Heat Transfer, **87**, pp. 426–427.
[21] Sparrow, E. M., Loeffler, A. L., and Hubbard, H. A., 1961, "Heat Transfer to Longitudinal Laminar Flow Between Cylinders," ASME J. Heat Transfer, **83**, pp. 415–422.
[22] Tyagi, V. P., 1966, "Laminar Forced Convection of a Dissipative Fluid in a Channel," ASME J. Heat Transfer, **46**, pp. 161–169.
[23] Shah, R. K., 1975, "Laminar Flow Friction and Forced Convection Heat Transfer in Ducts of Arbitrary Geometry," Int. J. Heat Mass Transfer, **18**(7-8), pp. 849–862.
[24] Richardson, S. M., 1980, "Leveque Solution for Flow in an Elliptical Duct," Lett. Heat Mass Transfer, **7**(5), pp. 353–362.
[25] Abdel-Wahed, R. M., and Attia, A. E., 1984, "Fully Developed Laminar Flow and Heat Transfer in an Arbitrarily Shaped Triangular Duct," Heat Mass Transfer, **18**(2), pp. 83–88.
[26] Maia, C. R. M., Aparecido, J. B., and Milanez, L. F., 2006, "Heat Transfer in Laminar Flow of Non-Newtonian Fluids in Ducts of Elliptical Section," Int. J. Therm. Sci., **45**(11), pp. 1066–1072.
[27] Tamayol, A., and Bahrami, M., 2010, "Laminar Flow in Microchannels With Noncircular Cross Section," ASME J. Fluids Eng., **132**(11), p. 111201.
[28] Cetin, B., Yazicioglu, A. G., and Kakac, S., 2008, "Fluid Flow in Microtubes With Axial Conduction Including Rarefaction and Viscous Dissipation," Int. Commun. Heat Mass Transfer, **35**(5), pp. 535–544.
[29] Tamayol, A., and Hooman, K., 2011, "Slip-Flow in Microchannels of Non-Circular Cross Section," ASME J. Fluids Eng., **133**(9), p. 092102.
[30] Jaklič, A., Leonardis, A., and Solina, F., 2000, *Segmentation and Recovery of Superquadrics*, Springer, New York.
[31] Kandlikar, S. G., Garimella, S., Li, D., Colin, S., and King, M. R., 2006, *Heat Transfer and Fluid Flow in Minichannels and Microchannels*, Elsevier Science & Technology, Oxford.
[32] Gad-El-Hak, M., 1999, "The Fluid Mechanics of Microdevices: The Freeman Scholar Lecture," J. Fluid Eng., **121**(1), pp. 7–33.
[33] White, F. M., 2003, *Fluid Mechanics*, McGraw-Hill Higher Education, Boston.
[34] Farlow, S. J., 1993, *Partial Differential Equations for Scientists and Engineer*, Dover Publication, Inc., New York.

[35] Tamayol, A., and Bahrami, M., 2010, "Parallel Flow Through Ordered Fibers: An Analytical Approach," ASME J. Fluids Eng., **132**(11), p. 114502.
[36] Sparrow, E. M., and Loeffler, A. L., 1959, "Longitudinal Laminar Flow Between Cylinders Arranged in Regular Array," AIChE J., **5**, pp. 325–330.
[37] Boyd, S., and Vandenberghe, L., 2004, *Convex Optimization*, Cambridge University Press, Cambridge.
[38] Kays, W., Crawford, M., and Weigand, B., 2005, *Convective Heat and Mass Transfer*, McGraw-Hill, New York, p. 118.
[39] Karniadakis, G., Beskok, A., and Aluru, N., 2005, *Microflows and Nanoflows*, Springer, New York.
[40] Incropera, F. P., and DeWitt, D. P., 1996, *Fundamentals of Heat and Mass Transfer*, John Wiley & Sons, New York.